

Machine learning for elastic-electrical cross-property modelling of  
sandstones

Phillip A. Cilli

Institute of Geoenergy Engineering, Heriot-Watt University,  
Edinburgh, EH14 4AS, UK

This manuscript is a non-peer reviewed preprint submitted to  
EarthArXiv. The content of subsequent versions may differ slightly.

Date submitted: 24/07/2022

# Machine learning for elastic-electrical cross-property modelling of sandstones

Phillip A. Cilli<sup>1\*</sup>

<sup>1</sup>Institute of Geoenergy Engineering,  
Heriot-Watt University, Edinburgh, EH14  
4AS, UK

**Correspondence**

Phillip A. Cilli, Institute of Geoenergy  
Engineering, Heriot-Watt University,  
Edinburgh, EH14 4AS, UK  
Email: p.cilli@hw.ac.uk

**Funding information**

This research has received no external  
funding.

The use of machine learning in rock physics has been rapidly increasing, however its application has not yet been popularised in cross-property modelling. The traditional mathematical models of cross-property modelling are often ineffective in the presence of clay or do not have any porosity terms due to the nature of their derivation. It is unclear what effect these two potentially problematic factors have on cross-property modelling accuracy. In this light, I use neural networks to model electrical properties from elastic measurements in public sandstone laboratory data and vice versa, and assess the importance of explicitly accounting for clay and porosity in cross-property modelling. I run three tests for both the forward and inverse problem: 1) including both clay volume fraction ( $V_{Clay}$ ) and porosity as neural network features; 2) including porosity but not  $V_{Clay}$  as a feature; and 3) including neither porosity nor  $V_{Clay}$  as a feature. I find modelling elastic properties from electrical measurements is least accurate when porosity is a feature but  $V_{Clay}$  is not. On the other hand, modelling electrical properties from elastic measurements is most accurate when porosity is a feature but  $V_{Clay}$  is not. Principal component analysis of the input features shows the first principal component is dominated by the electrical or elastic moduli and porosity, while the second and third are dominated by pressure and  $V_{Clay}$ . It is clear that the role of clay

and porosity in cross-property modelling is complex, however machine learning seems a promising way to improve our understanding of this complexity.

#### KEYWORDS

Machine learning, electrical, elastic, cross-property, modelling, neural network, rock physics

## 1 | INTRODUCTION

Machine learning methods are being rapidly adapted and developed in the field of rock physics, with notable progress in areas such as digital rock physics (e.g., Dvorkin et al. (2011); Saad et al. (2018); Miarelli and Della Torre (2021)) and pore- to laboratory or field scale property estimation (e.g., Gottschalk and Knight (2022); Dræge (2018); Menke et al. (2021)). While machine learning has been used for seismic rock physics inversion (e.g. Côte et al. (2020); Weinzierl and Wiese (2021); Downton et al. (2019)), facies and pore-type classification (e.g., Beloborodov et al. (2021); Sharifi et al. (2021); Zhang and Zhan (2017)), and well log generation and analysis (e.g., Akinnikawe et al. (2018); Rolon et al. (2009); Wu et al. (2018)), it has been ostensibly under-applied in cross-property modelling, including modelling the relationship between a rock's electrical and elastic properties.

These elastic-electrical cross-property relationships are of interest to the reservoir geosciences where joint electrical-elastic inversion using controlled source electromagnetic (CSEM) and seismic data can improve reservoir characterisation compared to the inversion of only CSEM or seismic data (Alcocer et al., 2013; Harris et al., 2009; Hu et al., 2009; Gehrmann et al., 2019). This is because, for the physical interpretation of these inversion results, we require understanding of the rock physics which link CSEM data to seismic data.

While Economou and Alaei (2016) presented a direct link from the electrical to elastic properties of rocks based on regression, most electrical-elastic models published to date relate the rock properties to one another analytically (Mavko et al., 2020). Carcione et al. (2007) proposed a suite of models by the substitution of electrical models into elastic models through the shared variable, porosity. This method of substitution through porosity was first performed by Sevostianov and Kachanov (2002), and has since been used by Werthmüller et al. (2013), and Han (2018), among others. Joint electrical-elastic modelling using a single model parameter has historically had mixed success (e.g., Wang and Gelius (2010); Han et al. (2011a); Jensen et al. (2013)), and Han et al. (2016) concluded that a new model was needed to relate the electrical and elastic properties of a rock with a single set of model parameters.

A model which satisfied these criteria was proposed by Cilli and Chapman (2021a), whereby the electrical and elastic Differential Effective Medium (DEM) models (e.g., Mendelson and Cohen (1982); Berryman (1992); Cilli and Chapman (2020)), both derived from first principles with consistent assumptions, were combined by substitution through porosity to form the cross-property DEM model. Like the other cross-property models derived from substitution through porosity (e.g., Carcione et al. (2007)), the cross-property DEM model has no porosity terms, yet unlike many other models, is derived from first principles. Derived from potential theory, the cross-property DEM model also extends to model the relationships between other physical properties, such as the electrical and thermal conductivities of composite materials (Cilli and Chapman, 2021b).

A strength of these porosity-free models is that they do not depend on porosity information away from well control. However, the idealised mathematical assumptions which allow us to remove porosity from these models may not always reflect reality and so we may be sacrificing model accuracy for the use of fewer model parameters; this

remains unclear.

The presence of clay can affect the physical properties of rocks, with the addition of only a small amount altering elastic (Han et al., 1986) and electrical (Waxman and Smits, 1968) properties significantly. To date, mathematical models such as the cross-property DEM model are not equipped to effectively account for the presence of clay. One can build clay mineralogy into the modelled background material, however choosing the correct solid mixing equation is not trivial, while selecting the correct clay moduli and conductivity is especially challenging and could only be done accurately by inverting for these hyper-parameters. Furthermore, the models are not generally derived to account for clay-related electrical phenomena such as the double-layer effect (Waxman and Smits, 1968).

In principle, the use of machine learning in electrical-elastic modelling allows us to constrain the effect of utilising clay and porosity information on modelling accuracy. Namely, we are able to use a neural network with the same hidden architecture to model electrical data from elastic measurements and vice versa, with and without clay and/or porosity features (inputs). Here I do this, performing electrical-elastic cross-property modelling using machine learning rather than the traditional mathematical model approach. In doing this, we see modelling error does not simply decrease as more modelling features are introduced. Rather, we observe a more complex relationship between the network features used and modelling error.

We commence by overviewing the data used in this study, followed by the electrical and elastic modelling methods and the details of the neural network implementation for modelling. I then present the obtained results in both electrical and elastic modelling, discuss principal component analyses and modelling errors, and draw conclusions.

## 2 | METHOD

### 2.1 | Data

I used the public laboratory dataset of Han et al. (2011b) to examine the forward and inverse electrical-elastic modelling of sandstones using neural networks. The dataset has been described in depth by Han et al. (2011b). Sandstone cores from multiple international localities with mixed mineralogies were tested in the laboratory, where  $V_p$ ,  $V_s$ , density, mineralogy, and electrical conductivity were measured among other properties. All measurements were taken at pressures 8, 15, 20, 26, 40, 60 MPa.

In this study, I model using measurements made on 63 of these cores. The statistics of the pertinent measured parameters across the cores are seen in Table 1, showing a large range in porosity, clay volume fraction, and electrical conductivity.

### 2.2 | Electrical Modelling

I ran three tests which used neural networks to model electrical conductivity from some of  $V_p$ ,  $V_s$ , density, pressure, porosity, and clay volume fraction measurements, training a different neural network for each test. The tests were designed to assess the modelling sensitivity to having porosity and clay volume fraction as network features. Table 2 summarises the features (inputs) and targets (outputs) in each test.

### 2.3 | Elastic Modelling

I also ran three tests which used neural networks to model  $V_p$  or three elastic properties from some of electrical conductivity measurements, pressure, porosity, and clay volume fraction. Like in the electrical modelling case, a different

**TABLE 1** Statistical description of 63 cores measured by Han et al. (2011b) used in this study.

Measurement	Min	Mean	Median	Max
$V_p$ (m/s)	2753	4346	4357	5540
$V_s$ (m/s)	1381	2573	2601	3320
$\rho$ (kg/m <sup>3</sup> )	2094	2450	2449	2664
$\sigma$ ( $\times 10^{-3}$ S/m)	4.98	94.7	52.0	847.5
$V_{Clay}$	0	0.10	0.10	0.28
$\phi$	0.02	0.12	0.12	0.28
$P$ (MPa)	8	28	23	60

$\rho$ , density;  $\phi$ , porosity;  $V_{Clay}$ , clay volume fraction;  $P$ , pressure;  $\sigma$ , electrical conductivity.

**TABLE 2** Features, targets, and RMS errors for the three electrical modelling tests. Note each test has one fewer feature than the previous. The RMS errors shown are calculated on the blind test data

Electrical test number	Features	Target	RMS error (S/m)
1	$V_p, V_s, \rho, \phi, V_{Clay}, P$	$\sigma$	$8.51 \times 10^{-3}$
2	$V_p, V_s, \rho, \phi, P$	$\sigma$	$8.17 \times 10^{-3}$
3	$V_p, V_s, \rho, P$	$\sigma$	$13.46 \times 10^{-3}$

$\rho$ , density;  $\phi$ , porosity;  $V_{Clay}$ , clay volume fraction;  $P$ , pressure;  $\sigma$ , electrical conductivity.

neural network was trained for each test and the tests were designed to assess the modelling sensitivity to having porosity and clay volume fraction as input features. Table 3 summarises the features and targets in each test. Elastic Test 1 entailed predicting  $V_p$ ,  $V_s$  and density, however, to avoid the optimisation problem being underdetermined, Elastic Tests 2 and 3 predicted only  $V_p$ .

## 2.4 | Neural network implementation

Machine learning was employed to model both electrical data from elastic measurements and elastic data from electrical measurements separately. In all modelling cases, the same multilayer perceptron architecture and optimisation parameters were used. The neural network was composed of an input layer with a variable number of features depending on the test, followed by 7 hidden layers with 100 neurons then one hidden layer with 50 neurons. The subsequent output layer had one or three targets depending on the test. All activation functions were hyperbolic tangent and a learning rate of  $10^{-3}$  was used. The loss function was mean squared error and the Adam (Kingma and Ba, 2014) optimisation algorithm was employed. All tests ran to 2000 epochs although convergence generally occurred in less than 1000.

For all six tests, twenty percent of all available data was randomly chosen and held aside as the blind test dataset. The remaining data was randomly split 60% : 40% into testing and validation datasets, respectively. Standard (Z-score) scaling was applied to data before feeding into the neural network.

**TABLE 3** Features, targets, and RMS errors for the three elastic modelling tests. Note each test has one fewer feature than the previous. Tests 2 and 3 only modelled  $V_p$  to ensure the problem was not underdetermined. The RMS errors shown are calculated on the blind test data.

Elastic test number	Features	Target(s)	$V_p$ RMS error (m/s)	$V_s$ RMS error (m/s)	$\rho$ RMS error (kg/m <sup>3</sup> )
1	$\sigma, \phi, V_{Clay}, P$	$V_p, V_s, \rho$	66.7	54.2	12.5
2	$\sigma, \phi, P$	$V_p$	258.9	N/A	N/A
3	$\sigma, P$	$V_p$	177.8	N/A	N/A

$\rho$ , density;  $\phi$ , porosity;  $V_{Clay}$ , clay volume fraction;  $P$ , pressure;  $\sigma$ , electrical conductivity.

## 3 | RESULTS

### 3.1 | Electrical Modelling Results

Figure 1 shows modelled conductivities from Electrical Tests 1 to 3, while Table 2 shows the modelling errors. From Table 2, it is clear that modelling with both porosity and clay volume fraction as features (Electrical Test 1) leads to reasonably accurate predictions (e.g., when compared to Table 2). However, it is interesting to observe that the modelling error is even lower when clay volume fraction is removed from the feature list (Electrical Test 2). As might be expected, the modelling error was highest when both clay volume fraction and porosity were omitted as features (Electrical Test 3).

We see in Figure 1 the measured-predicted electrical conductivity cross-plot, showing the smallest scatter in Electrical Test 2 and the largest in Electrical Test 3, as described statistically in Table 2. The misfits in measured and predicted conductivities shown in rows 2 to 4 of Figure 1 also reflect this, with the smallest visible scatter in Electrical Test 2 and the largest in Electrical Test 3.

### 3.2 | Elastic Modelling Results

Figure 2 shows modelled elastic properties from Elastic Tests 1 and Figure 3 shows modelled  $V_p$  from Elastic Tests 1-3, while Table 3 shows the modelling errors. Table 3 shows that modelling with both porosity and clay volume fraction as features (Elastic Test 1) leads to the most accurate predictions of  $V_p$ . Unlike the electrical case, however, the modelling error is highest when clay volume fraction is removed from the feature list but porosity remains (Elastic Test 2). The modelling error when both clay volume fraction and porosity are omitted as modelling features (Elastic Test 3) is significantly higher than when they are both included (Elastic Test 1).

## 4 | DISCUSSION

### 4.1 | Principal Component Analysis

Principal component analysis (e.g., Jolliffe and Cadima (2016)) can be used to further investigate the importance of clay and porosity in cross-property modelling. Table 4 shows the principal components of the features of Electrical Test 1 such that over 93% of the data's variance is explained. The first principal component, explaining 59% of the variance in the data, is most dependent on the rock's elastic properties as well as its porosity. The second and third components, which together explain 34% of the variance in the data, are both mostly dependent on the rock's clay

**TABLE 4** Principal components of the features of Electrical Test 1 such that over 93% of the data's variance is explained. Columns show the component value for each listed feature. Features of high importance to each principal component are shown in boldface.

Principal Component Number	EVR	$V_p$	$V_s$	$\rho$	$V_{Clay}$	$\phi$	$P$
1	0.59	<b>-0.50</b>	<b>-0.44</b>	<b>-0.50</b>	-0.23	<b>0.50</b>	-0.08
2	0.20	0.23	0.36	-0.20	<b>-0.53</b>	0.20	<b>0.67</b>
3	0.14	-0.16	-0.21	-0.03	<b>0.68</b>	0.05	<b>0.68</b>

EVR, Explained Variance Ratio;  $\rho$ , density;  $\phi$ , porosity;  $V_{Clay}$ , clay volume fraction;  $P$ , pressure.

**TABLE 5** Principal components of the features of Elastic Test 1 such that over 95% of the data's variance is explained. Columns show the component value for each listed feature. Features of high importance to each principal component are shown in boldface.

Principal Component Number	EVR	$\sigma$	$V_{Clay}$	$\phi$	$P$
1	0.54	<b>0.62</b>	-0.46	<b>0.63</b>	0.00
2	0.25	-0.04	-0.03	0.02	<b>1.00</b>
3	0.17	0.36	<b>0.88</b>	0.29	0.03

EVR, Explained Variance Ratio;  $\sigma$ , conductivity;  $\phi$ , porosity;  $V_{Clay}$ , clay volume fraction;  $P$ , pressure.

volume fraction and pressure.

Performing principal component analysis on the features of Elastic Test 1, Table 5 shows the corresponding principal components such that over 95% of the data's variance is explained. The first principal component explains 54% of the variance in the data and is most dependent on the rock's electrical conductivity as well as its porosity. The second principal component, which explains 25% of the variance in the data, is almost entirely dependent on pressure. The third principal component explains 17% of the data's variance and is highly dependent on the rock's clay volume fraction.

We can conclude from Tables 4 and 5 that the first principal component, which explains over 50% of the variance in each dataset, is primarily a function of elastic or electrical moduli and porosity, while the second and third principal components are predominantly functions of pressure and clay volume fraction.

## 4.2 | Modelling Error Analysis

We have observed that, in the case of electrical modelling, the error is lowest of all three scenarios when clay volume fraction is omitted from the list of features. However, we see the opposite occurring in the elastic modelling case, where the largest error in  $V_p$  estimation happens when clay volume fraction is omitted from the list of features. The presence of only a small amount of clay is known to change both the electrical and elastic properties of rocks significantly, so it could be these complex clay effects which lead to the observed, possibly unexpected result.

Another possibly reason why Electrical and Elastic Tests 2 have the lowest and highest modelling errors in their classes respectively could be the implementation of neural networks in modelling. In all 6 tests, the same neural network architecture was used. However, it is possible that modelling electrical properties would require a different

**TABLE 6** RMS coefficient of variation for all tests.

Test	RMS coefficient of variation (%)
Electrical 1	10.6
Electrical 2	10.2
Electrical 3	16.7
Elastic 1	1.5
Elastic 2	5.9
Elastic 3	4.0

neural network to modelling elastic properties to obtain the most accurate predictions of both. Indeed, every test may benefit from its own optimised neural network architecture and learning rate. Aware of these potential methodological shortcomings, I designed this experiment using a single network architecture and parameterisation regardless to reduce the number of independent variables and parameters, encouraging comparability of results and repeatability of the experiment.

Table 6 shows the RMS coefficient of variation or normalised RMS for every test, where the RMS coefficient of variation is defined here as the RMS error normalised by the mean of the measured dependent variable. Comparing coefficients of variation, we see the elastic modelling was an order of magnitude more accurate than the electrical modelling. This is interesting as the ratio of features to targets is lower in elastic modelling than in electrical. This asymmetry in modelling accuracy is notable and may have implications for the implementation of joint electrical-elastic modelling.

It is clear from Table 6 that including clay volume fraction as a feature leads to more accurate modelling of elastic properties (Elastic Test 1). This may be a benefit of neural network modelling over traditional mathematical methods, where accurately capturing the effects of clay can be notoriously difficult. As is often the case in physical modelling, one potential downside of using neural networks instead of mathematical models for cross-property modelling is having limited understanding of the physical processes being modelled. Therefore, in the case where we are focussed predominantly on making cross-property estimates, neural network modelling such as that shown here may be appropriate. However, in the case that a physical understanding of cross-property modelling is required, a first-principles model such as the cross-property DEM model is likely to be appropriate.

Another source of uncertainty in the elastic modelling part of this experiment is that Elastic Test 1 predicts three elastic properties and Tests 2 and 3 predict only one property. To assess the impact of having a different set of targets in the neural network and hence terms in the associated optimisation's objective function, I ran a fourth elastic test the same as Elastic Test 1, but with one target only:  $V_p$ . The results were similar to those of Elastic Test 1 (Tables 3 and 6), with a  $V_p$  RMS error of 60.2 m/s, and RMS coefficient of variation of 1.4%. Although the modelling in this fourth elastic test is marginally more accurate than Elastic Test 1, presumably because the optimisation is not fitting multiple variables simultaneously, the interpretation of this study's results remains unchanged.

## 5 | CONCLUSIONS

While mathematical models currently dominate cross-property modelling, they have their shortcomings due to physical inconsistencies or unrealistic assumptions. Some of these shortcomings can be avoided by machine learning

modelling at the cost of losing some understanding of the underlying physics. Using machine learning can lead to the effective modelling of electrical properties from elastic measurements and vice versa, but the role of clay and porosity in this modelling is complex and still far from understood. Principal component analysis tells us that moduli and porosity are of primary importance while pressure and clay volume fraction are of secondary importance in explaining variance in the examined, public dataset. Ultimately, we can conclude that machine learning and data analytical techniques show promise in better understanding the roles of clay and porosity in cross-property relations.

## acknowledgements

The author would like to thank Colin MacBeth for his support and thank Angus Best and Tongcheng Han for providing the experimental data used.

## data availability

The data used in this paper are available in Han et al. (2011b) at <https://doi.org/10.1111/j.1365-2478.2010.00940.x>.

## references

- Akinnikawe, O., Lyne, S. and Roberts, J. (2018) Synthetic well log generation using machine learning techniques. In *SPE/AAPG/SEG Unconventional Resources Technology Conference*. OnePetro.
- Alcocer, J. E., García, M. V., Soto, H. S., Baltar, D., Paramo, V. R., Gabrielsen, P. T. and Roth, F. (2013) Reducing uncertainty by integrating 3D CSEM in the Mexican deep-water exploration workflow. *First Break*, **31**, 75–79.
- Beloborodov, R., Gunning, J., Pervukhina, M., Waters, K. and Huntbatch, N. (2021) Rock-physics machine learning toolkit for joint litho-fluid facies classification and compaction modeling. *The Leading Edge*, **40**, 742–750.
- Berryman, J. G. (1992) Single-scattering approximations for coefficients in Biot's equations of poroelasticity. *The Journal of the Acoustical Society of America*, **91**, 551–571.
- Carcione, J. M., Ursin, B. and Nordskog, J. I. (2007) Cross-property relations between electrical conductivity and the seismic velocity of rocks. *Geophysics*, **72**, E193–E204.
- Cilli, P. A. and Chapman, M. (2020) The power-law relation between inclusion aspect ratio and porosity: Implications for electrical and elastic modeling. *Journal of Geophysical Research: Solid Earth*, **125**, 1–25.
- (2021a) Linking elastic and electrical properties of rocks using cross-property dem. *Geophysical Journal International*, **225**, 1812–1823.
- (2021b) Linking electrical and thermal conductivity through cross-property inclusion modelling. *Materials Letters: X*, **12**, 100101.
- Côrte, G., Dramsch, J., Amini, H. and MacBeth, C. (2020) Deep neural network application for 4d seismic inversion to changes in pressure and saturation: Optimizing the use of synthetic training datasets. *Geophysical Prospecting*, **68**, 2164–2185.
- Downton, J., Collet, O. and Colwell, T. (2019) Rock-physics based augmented machine learning for reservoir characterization. In *EAGE Subsurface Intelligence Workshop*, vol. 2019, 1–5. European Association of Geoscientists & Engineers.
- Dræge, A. (2018) A new concept—fluid substitution by integrating rock physics and machine learning. *First Break*, **36**, 31–39.
- Dvorkin, J., Derzhi, N., Diaz, E. and Fang, Q. (2011) Relevance of computational rock physics. *Geophysics*, **76**, E141–E153.

- Economou, D. and Alaei, B. (2016) Direct elastic properties to resistivity transforms. *Geophysics*, **81**, IM109–IM118.
- Gehrmann, R. A., Schnabel, C., Engels, M., Schnabel, M. and Schwalenberg, K. (2019) Combined interpretation of marine controlled source electromagnetic and reflection seismic data in the German North Sea: A case study. *Geophysical Journal International*, **216**, 218–230.
- Gottschalk, I. and Knight, R. (2022) The development of a machine-learning approach to construct a field-scale rock-physics transform. *Geophysics*, **87**, MR35–MR48.
- Han, D.-h., Nur, A. and Morgan, D. (1986) Effects of porosity and clay content on wave velocities in sandstones. *Geophysics*, **51**, 2093–2107.
- Han, T. (2018) Joint elastic-electrical properties of artificial porous sandstone with aligned fractures. *Geophysical Research Letters*, **45**, 3051–3058.
- Han, T., Best, A. I., MacGregor, L. M., Sothcott, J. and Minshull, T. A. (2011a) Joint elastic-electrical effective medium models of reservoir sandstones. *Geophysical Prospecting*, **59**, 777–786.
- Han, T., Best, A. I., Sothcott, J. and MacGregor, L. M. (2011b) Joint elastic-electrical properties of reservoir sandstones and their relationships with petrophysical parameters. *Geophysical Prospecting*, **59**, 518–535.
- Han, T., Clennell, M. B., Cheng, A. C. H. and Pervukhina, M. (2016) Are self-consistent models capable of jointly modeling elastic velocity and electrical conductivity of reservoir sandstones? *Geophysics*, **81**, D377–D382.
- Harris, P., Du, Z., MacGregor, L., Olsen, W., Shu, R. and Cooper, R. (2009) Joint interpretation of seismic and csem data using well log constraints: An example from the Luva field. *First Break*, **27**.
- Hu, W., Abubakar, A. and Habashy, T. M. (2009) Joint electromagnetic and seismic inversion using structural constraints. *Geophysics*, **74**, R99–R109.
- Jensen, E. H., Gelius, L.-J., Johansen, T. A. and Wang, Z. (2013) Consistent joint elastic-electrical differential effective-medium modelling of compacting reservoir sandstones. *Geophysical Prospecting*, **61**, 788–802.
- Jolliffe, I. T. and Cadima, J. (2016) Principal component analysis: a review and recent developments. *Philosophical Transactions of the Royal Society A: Mathematical, Physical and Engineering Sciences*, **374**, 20150202.
- Kingma, D. P. and Ba, J. (2014) Adam: A method for stochastic optimization. *arXiv preprint arXiv:1412.6980*.
- Mavko, G., Mukerji, T. and Dvorkin, J. (2020) *The rock physics handbook*. Cambridge University Press.
- Mendelson, K. S. and Cohen, M. H. (1982) The effect of grain anisotropy on the electrical properties of sedimentary rocks. *Geophysics*, **47**, 257–263.
- Menke, H. P., Maes, J. and Geiger, S. (2021) Upscaling the porosity–permeability relationship of a microporous carbonate for Darcy-scale flow with machine learning. *Scientific Reports*, **11**, 1–10.
- Miarelli, M. and Della Torre, A. (2021) Workflow development to scale up petrophysical properties from digital rock physics scale to laboratory scale. *Transport in Porous Media*, **140**, 459–492.
- Rolon, L., Mohaghegh, S. D., Ameri, S., Gaskari, R. and McDaniel, B. (2009) Using artificial neural networks to generate synthetic well logs. *Journal of Natural Gas Science and Engineering*, **1**, 118–133.
- Saad, B., Negara, A. and Syed Ali, S. (2018) Digital rock physics combined with machine learning for rock mechanical properties characterization. In *Abu Dhabi International Petroleum Exhibition & Conference*. OnePetro.
- Sevostianov, I. and Kachanov, M. (2002) Explicit cross-property correlations for anisotropic two-phase composite materials. *Journal of the Mechanics and Physics of Solids*, **50**, 253–282.

- Sharifi, J., Ghiasi-Freez, J. and Taheri, S. (2021) Pore type classification using multi-class classifiers: Application in rock physics modelling. In *82nd EAGE Annual Conference & Exhibition*, vol. 2021, 1–5. European Association of Geoscientists & Engineers.
- Wang, Z. and Gelius, L.-J. (2010) Electric and elastic properties of rock samples: A unified measurement approach. *Petroleum Geoscience*, **16**, 171–183.
- Waxman, M. H. and Smits, L. J. M. (1968) Electrical conductivities in oil-bearing shaly sands. *Society of Petroleum Engineers Journal*, **8**, 107–122.
- Weinzierl, W. and Wiese, B. (2021) Deep learning a poroelastic rock-physics model for pressure and saturation discrimination. *Geophysics*, **86**, MR53–MR66.
- Werthmüller, D., Ziolkowski, A. and Wright, D. (2013) Background resistivity model from seismic velocities. *Geophysics*, **78**, E213–E223.
- Wu, P.-Y., Jain, V., Kulkarni, M. S. and Abubakar, A. (2018) Machine learning-based method for automated well-log processing and interpretation. In *2018 SEG International Exposition and Annual Meeting*. OnePetro.
- Zhang, L. and Zhan, C. (2017) Machine learning in rock facies classification: An application of xgboost. In *International Geophysical Conference, Qingdao, China, 17-20 April 2017*, 1371–1374. Society of Exploration Geophysicists and Chinese Petroleum Society.

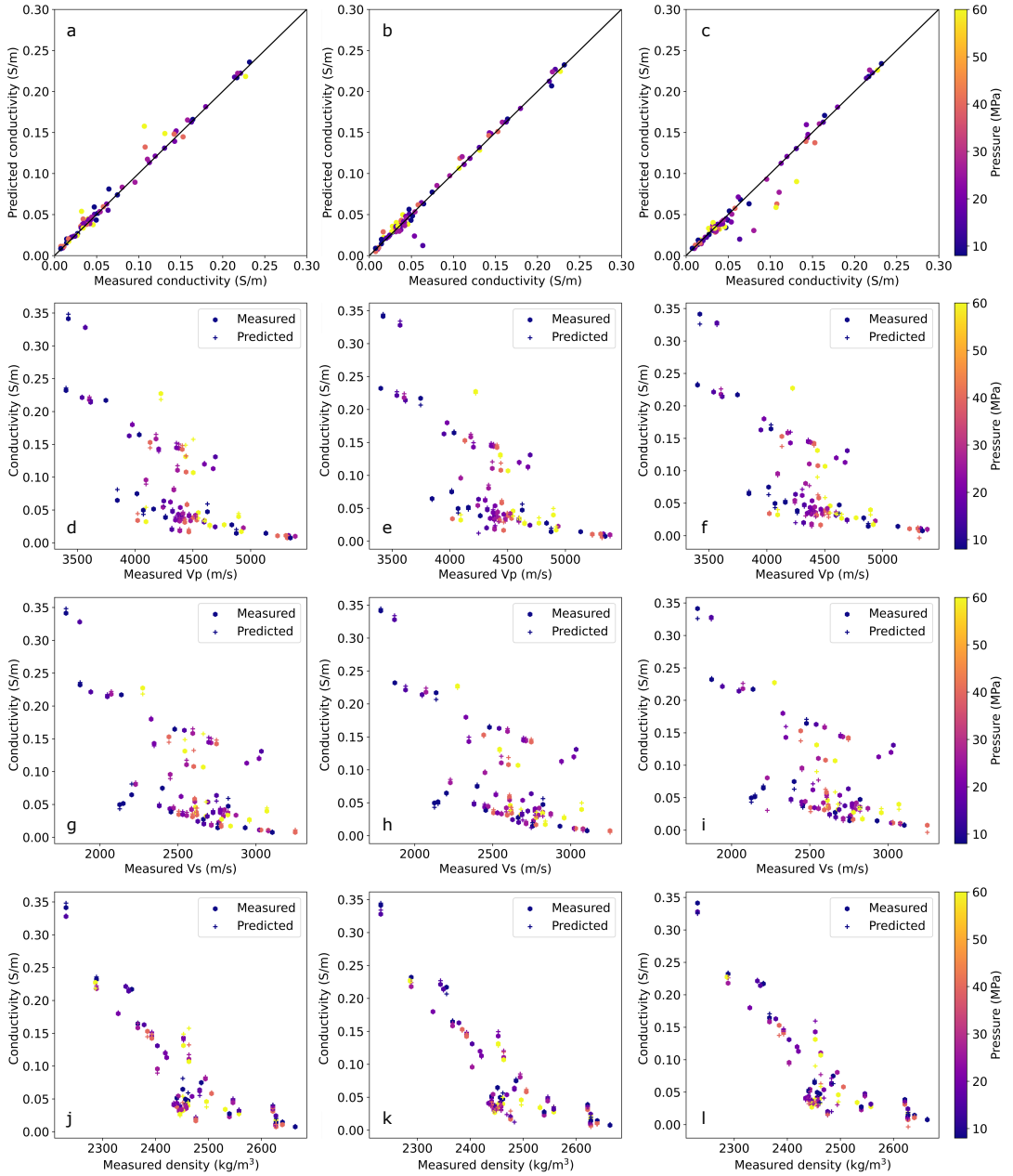


**FIGURE 1** Conductivities modelled from elastic measurements. Columns show three electrical tests: Left) Electrical Test 1: Including porosity and clay volume fraction; Centre) Electrical Test 2: Including porosity but no clay volume fraction; Right) Electrical Test 3: Including neither porosity nor clay volume fraction. The top row (a-c) shows cross-plots of measured and predicted conductivity and the 1:1 line. The second row (d-f) shows measured and modelled conductivity as a function of measured Vp, while the third row (g-i) and fourth row (j-l) show the measured and modelled conductivity as functions of measured Vs and density respectively.

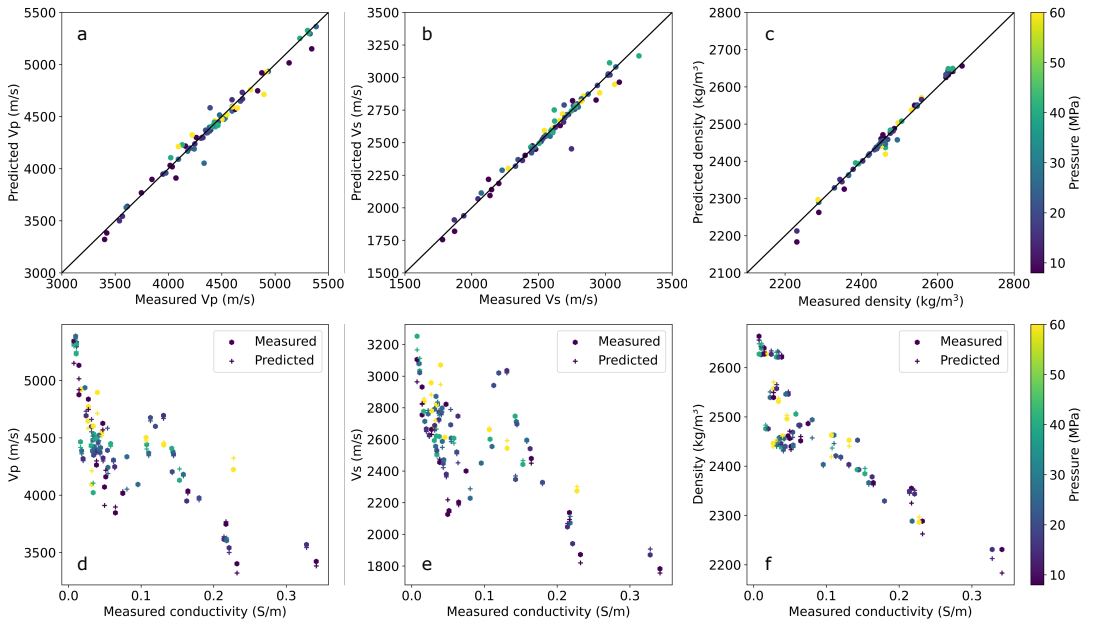


**FIGURE 2** Elastic properties modelled from electrical measurements using both porosity and clay volume fraction as features (Elastic Test 1). The top row (a-c) shows cross-plots of measured and predicted a)  $V_p$ , b)  $V_s$ , and c) density, as well as the 1:1 line. The second row shows measured and modelled d)  $V_p$ , e)  $V_s$ , and f) density as a function of measured conductivity.

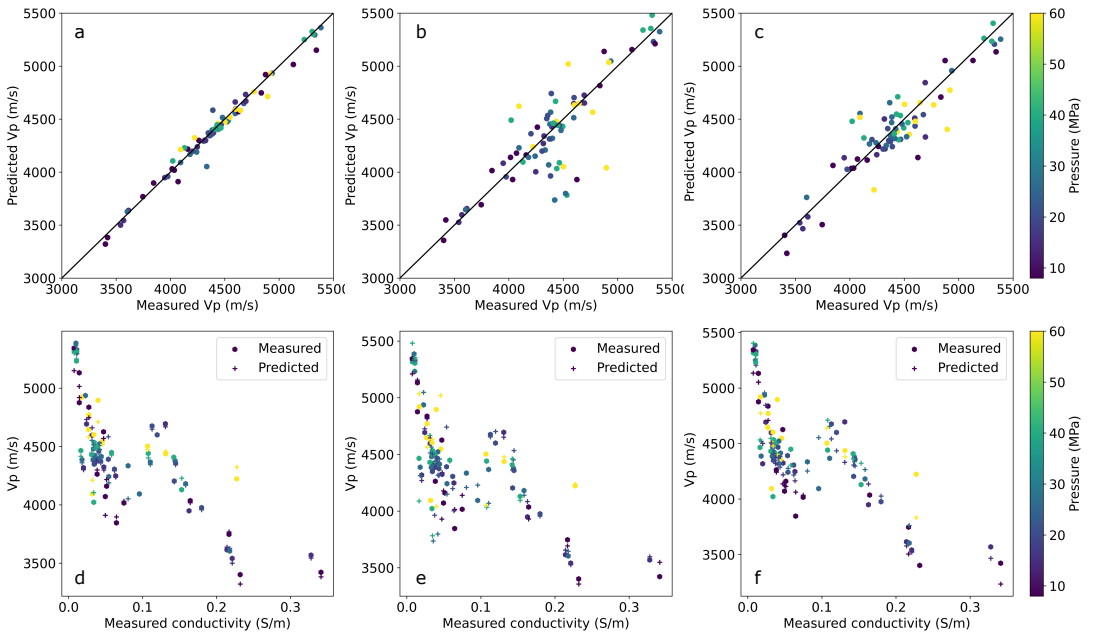


**FIGURE 3** Vp modelled from electrical measurements. Columns show three elastic tests: Left) Elastic Test 1: Including porosity and clay volume fraction; Centre) Elastic Test 2: Including porosity but no clay volume fraction; Right) Elastic Test 3: Including neither porosity nor clay volume fraction. The top row (a-c) shows cross-plots of measured and predicted Vp and the 1:1 line. The second row (d-f) shows measured and modelled Vp as a function of measured conductivity. Note a) and d) are also shown in Figure 2.